Environ. Sci. Technol. **2006**, *40,* 263−271

Anion Adsorption on Oxide Surfaces: Inclusion of the Water Dipole in Modeling the Electrostatics of Ligand Exchange

DIMITRI A. SVERJENSKY* AND KEISUKE FUKUSHI

Department of Earth and Planetary Sciences, The Johns Hopkins University, Baltimore, Maryland 21218

Adsorption of aqueous anions, such as sulfate, arsenite, and oxalate, to oxide surfaces is important in the retardation of toxic species in the environment, but predicting the surface speciation as a function of environmental parameters is a major challenge. Recent laboratory spectroscopic studies defining surface speciation must be integrated with surface complexation models. However, the latter have neglected the electrostatic work of desorption of water dipoles in treating anion adsorption by ligand exchange. Taking this effect into account permits close quantitative description of anion adsorption and the prediction of anion surface speciation as a function of pH, ionic strength, and surface coverage in agreement with spectroscopic results.

Introduction

Aqueous anions, from sulfate and arsenite to anionic functional groups on biomolecules, adsorb on the electrically charged surfaces of oxides, influencing the mobilities of toxic species in the environment (*1*), weathering of minerals in the soil zone (*2*), interactions of microbes, plants, and fungi with mineral surfaces (*3*), binding of medical implants in the human body (*4*), and theories about the origin of life (*5*). Recently, increasing numbers of in situ infrared and X-ray spectroscopic studies have definitively established how some aqueous anions bind to oxides, including information on the structure and number of surface species, their protonation states, and even the proportion of inner- to outer-sphere surface complexes (*6*−*10*). However, the integration of these experimental results with long-standing theoretical surface complexation models used for the description of bulk adsorption and electrokinetic data has become a major challenge (*11*−*14*). With the increasing interest in the use of surface complexation models in a predictive mode to facilitate analysis of the migration of nuclear and other toxic wastes in the environment (*15, 16*), it is imperative that the identity of the surface chemical species in the models reflect the spectroscopic results (*12, 17, 18*).

Model predictions of adsorption as a function of pH, ionic strength, and surface coverage are strongly influenced by how the electrostatic work of adsorption is specified (*12, 17, 19*−*22*). Typically the electrostatic work in adsorption reactions is specified by some form of the relationship $\delta w = -F\Delta\psi_r$, where $F = 96\,485$ C·mol^{-1} represents the Faraday constant and $\Delta\psi_r$(*V*) represents the change in potential associated with the *r*th reaction. For over 30 years, $\Delta\psi_r$ has been formulated in surface complexation models by taking account only of the ions moving to or from the surface (*19, 23*−*28*). But the movement of dipolar molecules to or from a charged surface also involves electrostatic work (*29*); however, this work has never been included in surface complexation models. In particular, inner-sphere anion adsorption proceeds by a ligand-exchange mechanism, which involves desorption of water dipoles (*28, 30, 31*), but the electrostatic work of water dipole desorption has not been investigated.

We report a new theoretical modification of the triple-layer model (TLM) of surface complexation that takes account of the electrostatic work associated with desorption of water dipoles during anion adsorption by ligand-exchange reactions. It will be shown below that the magnitude of the electrostatic work associated with this dipole modification is substantial and depends only on the stoichiometry of the surface reaction. No additional fitting parameters are involved. As a result, the sensitivity of the triple-layer model to predicting alternate speciation schemes is enhanced, enabling integration of the number and protonation states of the adsorbed anions established in spectroscopic studies with models of adsorption data. Furthermore, the models permit prediction of the proportions of inner- to outer-sphere surface complexes which compare favorably with spectroscopic results and prediction of ζ-potentials in qualitative agreement with electrokinetic data. We illustrate the model capabilities by application to three environmentally important anions, sulfate (SO_4^{2-}), arsenite (AsO_3^{3-}), and oxalate ($C_2O_4^{2-}$), for which spectroscopic results have defined the surface species, and for which there are adsorption data extending over wide ranges of pH, ionic strength, and surface coverage.

Theory

Anion adsorption by a ligand-exchange mechanism involves the release of a water dipole from the adsorption site (*28*, *30*, *31*). A diagrammatic representation of such a water dipole before its desorption is shown in Figure 1. The two principal planes of adsorption in the triple-layer model are the 0-plane and the β-plane, where protons and electrolyte ions adsorb, respectively. In Figure 1, it is assumed that proton adsorption has resulted in the water dipole located on the 0-plane. The magnitude of the electrostatic work associated with desorption of a mole of such water dipoles from the 0-plane (*29*) is given by

$$\delta w = p_{H_2O}(X\cos\alpha)N_A = p_{H_2O}\left(\frac{\sigma_0}{\epsilon_{H_2O}\epsilon_0}\right)N_A \qquad (1)$$

where p_{H_2O}(C·m) represents the dipole moment of water at the site, X(V·m^{-1}) represents the magnitude of the electric field, α represents the angle between the dipole unit vector and the electric field vector (α = 0 in Figure 1), σ_0 (C·m^{-2}) represents the charge on the 0-plane, ϵ_{H_2O} represents the dielectric constant of water at the surface site, $\epsilon_0 = 8.854 \times 10^{-12}$C^2·J^{-1}·m^{-1}, and $N_A = 6.023 \times 10^{23}$mol^{-1}

In the triple-layer model, the surface charge at the 0-plane (σ_0) and the potentials at the 0- and β-planes (ψ_0 and ψ_β, respectively) are related by the integral capacitance C_1(F·m^{-2}), where $\sigma_0 = C_1(\psi_0 - \psi_\beta)$. Substituting for σ_0 in eq 1 results in

$$\delta w = k_{H_2O}(\psi_0 - \psi_\beta) \qquad (2)$$

* Corresponding author e-mail: sver@jhu.edu.

10.1021/es051521v CCC: $33.50
Published on Web 12/01/2005

where

$$k_{H_2O} = \frac{p_{H_2O} C_1 N_A}{\epsilon_{H_2O} \epsilon_0} \quad (3)$$

It can be seen in eq 2 that k_{H_2O} relates the electrostatic work of desorption of water dipoles to the difference in potentials between the 0- and the β-planes. The units of k_{H_2O} are C·mol^{-1}. Equation 2 closely parallels the corresponding relationship traditionally used for the electrostatic work of adsorption/desorption of ions, i.e., $\delta w = -F\Delta\psi_r$. It is therefore of interest to evaluate k_{H_2O} relative to F. Considerable uncertainty is associated with evaluating k_{H_2O} because specific values for the interfacial properties of water, such as ϵ_{H_2O} and p_{H_2O}, are not well known. As a first approximation, we have evaluated k_{H_2O} using estimates of $\epsilon_{H_2O} = 6$ (*29*), $p_{H_2O} = 2.9$ D, the dipole moment of bulk water (*32*), and a typical value for $C_1 = 1.0$ F·m^{-2} (*33*). These approximations result in $k_{H_2O} \approx 109\,000$ C·mol^{-1}, which is within 13% of the Faraday constant ($F = 96\,485$ C·mol^{-1}). Given the uncertainties in the interfacial properties of water, we propose setting $k_{H_2O} \approx F$, thereby evaluating the dipole contribution to the electrostatic work of ligand exchange by

$$\delta w \approx F(\psi_0 - \psi_\beta) \quad (4)$$

per mole of water in the reaction. Although eq 4 represents an extreme simplification of the expression in eq 1, it has widespread applicability, as will be demonstrated with the examples below. It follows from eq 4 that if n moles of water are desorbed during an inner-sphere ligand-exchange reaction, the electrostatic work resulting solely from the dipole desorption can be expressed in equilibrium constant form by

$$K_{dipole} = 10^{-nF(\psi_0 - \psi_\beta)/2.303RT} \quad (5)$$

The overall change in potential for the rth anion adsorption reaction by ligand exchange, $\Delta\psi_r$, traditionally formulated based only on the ions in the reaction, can thus be corrected very simply by adding $-n(\psi_0 - \psi_\beta)$ to take into account the contribution from desorption of water dipoles.

Application and Discussion

As a first example of the application of the dipole modification to the TLM, we consider sulfate adsorption on goethite, of which many studies have been made (*34*). In situ attenuated total reflection-Fourier-transform IR spectroscopy (ATR−FTIR) measurements (*7, 35*) have established that sulfate forms a mononuclear, monodentate inner-sphere complex and an outer-sphere complex on goethite. We used this information to construct a surface complexation model constrained by adsorption data referring to wide ranges of pH, ionic strength, and surface coverage (*36*) shown in Figure 2a. The solid curves in Figure 2a were generated by regression of the experimental data shown using two sulfate surface complexes. First, the reaction forming a mononuclear, monodentate inner-sphere complex is represented by

$$>\!FeOH + H^+ + SO_4^{2-} = >\!FeOSO_3^- + H_2O \quad (6)$$

and

$$K = \frac{a_{>FeOSO_3^-}\, a_{H_2O}}{a_{>FeOH} a_{H^+}\, a_{SO_4^{2-}}} 10^{F(\Delta\psi_r)/2.303RT} \quad (7)$$

where $10^{F(\Delta\psi_r)/2.303RT}$ represents the equilibrium constant expression of the electrostatic work done in an electric field when species in the reaction move on or off the charged

WATER DIPOLE IN THE TRIPLE LAYER MODEL

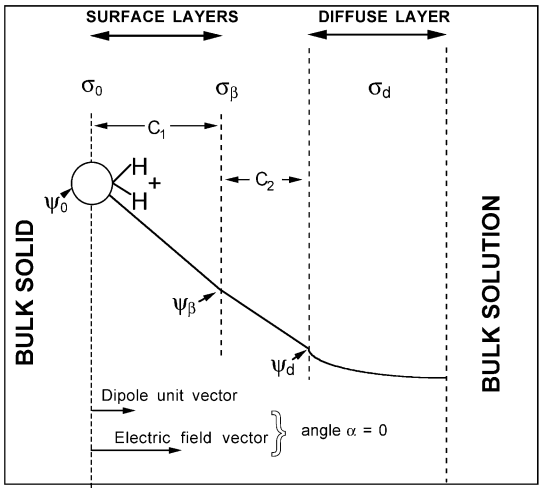

FIGURE 1. Diagrammatic representation of a water dipole adsorbed at a surface site in the triple-layer model of surface complexation. For simplicity, no other species are depicted. It is assumed that the surface site is positively charged. Consequently, the water molecule is depicted in the "flip up" position (*29*) and the water dipole unit vector points toward the solution, as does the electric field vector. The two surface adsorption planes in the triple-layer model are the 0-plane and the β-plane, where protons and electrolyte ions adsorb, respectively. These planes are associated with the charges and potentials σ_0, ψ_0 and σ_β, ψ_β, respectively.

surface. In the present study, $\Delta\psi_r$ is evaluated using both ions and dipoles: the ions experience changes in potential relative to the bulk solution depending on which plane they are placed, and the water dipole experiences an additional change in potential equal to $-n(\psi_0 - \psi_\beta)$ from eq 5. For the reaction in eq 6, the modified TLM results in

$$\Delta\psi_r = \psi_0 - 2\psi_\beta - (\psi_0 - \psi_\beta) = -\psi_\beta \quad (8)$$

In eq 8, the three terms in the middle correspond to changes in the potentials experienced by the H^+ ion adsorbing to the 0-plane, the SO_4^{2-} ion adsorbing to the β-plane, and the H_2O desorbing from the 0-plane, respectively.

Second, the reaction forming an outer-sphere complex is represented by

$$2\,>\!FeOH + 2H^+ + SO_4^{2-} = (>\!FeOH_2^+)_2\_SO_4^{2-} \quad (9)$$

and

$$K = \frac{a_{(>FeOH_2^+)_2\_SO_4^{2-}}}{a_{>FeOH}^2\, a_{H^+}^2\, a_{SO_4^{2-}}} 10^{2F(\psi_0 - \psi_\beta)/2.303RT} \quad (10)$$

Here, $\Delta\psi_r$ is expressed solely in terms of the ions in the reaction. It can be seen in Figure 2a that the combination of reactions 6 and 9 results in a close description of the experimental adsorption data. An independent test of the model can be made by comparison of predictions of the relative contributions of the inner- and outer-sphere complexes with spectroscopic results. It can be seen in Figure 2b−d that the proportion of the outer-sphere complex is predicted to increase as a function of pH and decrease with ionic strength and surface coverage. All three of these predicted model variations have been detected spectroscopically (*7, 35*), providing strong support to the dipole model.

Without the dipole modification to $\Delta\psi_r$ in eq 8, the model fit and predictions are quite different. In a TLM that takes into account ions only, eq 8 would give $\Delta\psi_r = \psi_0 - 2\psi_\beta$ for

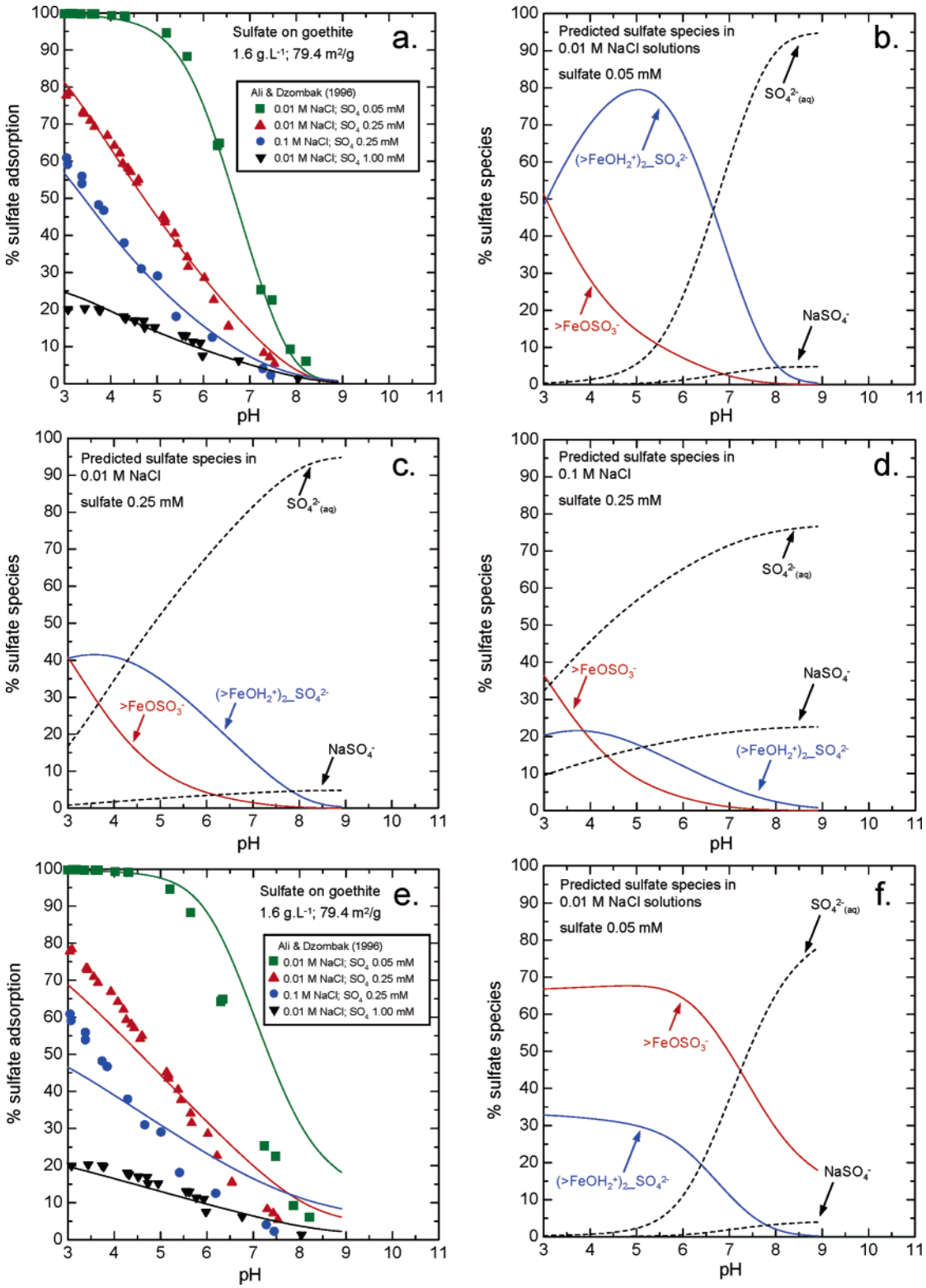

FIGURE 2. Sulfate adsorption on goethite. The curves in a–d were calculated with the dipole modification of the TLM using sulfate surface species given in eqs 6–10 and log $*K^0_{>FeOSO_3^-} = 9.1$ ($\Delta\psi_r = -\psi_\beta$), log $*K^0_{(>FeOH_2^+)2\_SO_4^{2-}} = 21.6$ ($\Delta\psi_r = 2\psi_0 - 2\psi_\beta$), log $*K_1^0 = 4.9$, log $*K_2^0 = 11.1$, log $*K^0_{Na^+} = -7.8$, log $*K^0_{Cl^-} = 8.0$, and $C_1 = 1.15$ F·m^{-2}. The curves in e and f were calculated with the traditional TLM using log $*K^0_{(>FeOH_2^+)2\_SO_4^{2-}} = 12.5$ ($\Delta\psi_r = \psi_0 - 2\psi_\beta$) and log $*K^0_{(>FeOH_2^+)2\_SO_4^{2-}} = 21.6$ (see text). The surface protonation and electrolyte adsorption parameters were calculated from a previous analysis of surface titration data (*45*) to be consistent with the site density of 2.5 sites·nm^{-2} (based on preliminary fits as a function of suface coverage). (a) Sulfate adsorption as a function of pH, ionic strength, and surface coverage. The curves represent regression fits of the experimental data plotted as symbols (*46*). (b–d) Predicted model sulfate surface and aqueous speciation as functions of pH, ionic strength, and surface coverage. The outer- and inner-sphere sulfate surface complexes are approximately equal in abundance only at low pH. The proportion of outer-sphere complex increases with pH, but decreases with increasing ionic strength and surface coverage consistent with ATR–FTIR results (*7, 35*). (e,f) The curves represent traditional TLM calculations which differ from those in a–d solely through the use of a different electrostatic factor for the mononuclear sulfates complex and different magnitudes of log *K* values (as noted above).

a mononuclear, monodentate complex on the β-plane. The resulting adsorption model curves and predicted speciation are shown in Figure 2e,f. It can be seen in Figure 2e that the model curves do not fit the data adequately. In Figure 2f, the relative abundances of the predicted species are inconsistent with spectroscopic results. The large differences between panels e and f in Figure 2, compared to panels a and b, are due solely to the use of a different electrostatic factor and log K value for eq 7: $\Delta\psi_r = \psi_0 - 2\psi_\beta$ for a TLM with no dipole contribution compared to $\Delta\psi_r = -\psi_\beta$ with a dipole contribution. It is clear that taking into account the electrostatics of water dipole desorption has a large effect on the performance of the surface complexation model.

It should be noted that in the regression calculations, which generated the curves shown in Figure 2a, the two surface complexes of sulfate discussed above are necessary when using the dipole modification of the TLM. One complex alone is not sufficient to fit the data. This result is independent of the spectroscopic constraints. It contrasts with the charge distribution (CD) model of sulfate adsorption on goethite which can fit adsorption data equally well with either an inner-sphere complex or both inner- and outer-sphere complexes (*37*). The relative insensitivity of the CD approach to using either one or two sulfate surface species is likely a consequence of splitting the surface charge between two planes when the splitting factor becomes a fit parameter in addition to the equilibrium constant of adsorption. Even when both inner- and outer-sphere sulfate species are used, the CD model does not predict the relative ionic strength dependence of the two species established in the spectroscopic studies (*37*). As noted above, the dipole modification of the TLM does predict the correct relative ionic strength dependence for the inner- and outer-sphere sulfate species (Figure 2c,d). Additionally, we have found that eqs 6−10 are closely consistent with many other sets of sulfate/goethite data, including proton surface charge in sulfate solutions (*38, 39*) and proton uptake as a function of sulfate adsorption (*37*). Finally, dipole model predictions of the ζ potential for goethite in sulfate solutions (assuming $\zeta = \psi_d$) show little displacement of the isoelectric point, consistent with extrapolation of trends in electrophoretic mobility data with pH (*40*).

As a second example of the application of the dipole modification to the TLM, we consider arsenite adsorption on β-Al(OH)$_3$ (bayerite). XAFS and XANES measurements (*6*) have established that arsenite forms a binuclear, bidentate inner-sphere complex and an outer-sphere complex on this alumina. We used this information to construct a surface complexation model consistent with adsorption data as a function of pH and ionic strength. The solid curves in Figure 3a were generated by regression of the experimental data shown using two arsenite surface complexes. The first complex used was represented by

$$2\ {>}\mathrm{AlOH} + \mathrm{As(OH)_3}^0 = ({>}\mathrm{AlO})_2\mathrm{As(OH)}^0 + 2\mathrm{H_2O} \quad (11)$$

and

$$K = \frac{a_{({>}\mathrm{AlO})_2\mathrm{As(OH)}^0} a_{\mathrm{H_2O}}{}^2}{a_{{>}\mathrm{AlOH}}{}^2 a_{\mathrm{As(OH)_3}^0}} 10^{F(\Delta\psi_r)/2.303RT} \quad (12)$$

where

$$\Delta\psi_r = 2\psi_0 - 2\psi_\beta - 2(\psi_0 - \psi_\beta) = 0 \quad (13)$$

In eq 13, the three terms in the middle correspond to changes in the potentials experienced by the $2H^+$ ions adsorbing to the 0-plane, the $AsO_2(OH)^{2-}$ ion adsorbing to the β-plane, and the $2H_2O$ desorbing from the 0-plane, respectively. The second complex used was an outer-sphere complex represented by

$${>}\mathrm{AlOH} + \mathrm{As(OH)_3^0} = {>}\mathrm{AlOH_2^+}\_\mathrm{AsO(OH)_2^-} \quad (14)$$

and

$$K = \frac{a_{{>}\mathrm{AlOH_2^+}\_\mathrm{AsO(OH)_2^-}}}{a_{{>}\mathrm{AlOH}} a_{\mathrm{As(OH)_3^0}}} 10^{F(\psi_0 - \psi_\beta)/2.303RT} \quad (15)$$

It can be seen in Figure 3a that the combination of reactions 11 and 14 results in a close description of the experimental adsorption data. Furthermore, it can be seen in Figure 3b,c that the predicted proportion of the outer-sphere complex increases with pH and decreases with ionic strength, which agrees with the variations reported in the X-ray study. In addition, it can be seen in Figure 3d that the predicted ratio of outer- to inner-sphere complexes is in close agreement with the XANES result (*6*). Finally, model predictions of the ζ potential for alumina in arsenite solutions (assuming $\zeta = \psi_d$) show a very small displacement of the isoelectric point, consistent with extrapolation of trends in electrophoretic mobility data with pH (*6, 14*).

Without the dipole modification to $\Delta\psi_r$ in eq 13, the model fit and predictions are quite different. In a TLM that takes account of ions only, eq 13 would give $\Delta\psi_r = 2\psi_0 - 2\psi_\beta$ for a binuclear, bidentate complex on the β-plane. The resulting adsorption model curves and predicted speciation are shown in Figure 3e,f. It can be seen in Figure 3e that the model curves are grossly inconsistent with the adsorption data. In Figure 3f, the relative abundances of the predicted species are also inconsistent with spectroscopic results. The large differences between panels e and f in Figure 3 compared with panels a and b are due solely to the use of $\Delta\psi_r = 2\psi_0 - 2\psi_\beta$ (no dipole contribution) versus $\Delta\psi_r = 0$ (with dipole contribution) as well as to the use of different log K values. Again it is clear that taking into account the electrostatics of water dipole desorption has a very large effect on the performance of the surface complexation model.

As a third example of the application of the dipole modification to the TLM, we consider oxalate adsorption on goethite (*8*). ATR−FTIR measurements have established that oxalate forms a mononuclear, bidentate inner-sphere complex and an unprotonated outer-sphere complex on goethite (*8*). We used this information to construct a surface complexation model consistent with the adsorption data as a function of pH and ionic strength. In principle, mononuclear bidentate complexes can be represented with the TLM in two ways:

$${>}\mathrm{Fe(OH)_2} + 2\mathrm{H^+} + \mathrm{C_2O_4^{2-}} = {>}\mathrm{FeO_2C_2O_2^0} + 2\mathrm{H_2O} \quad (16)$$

and

$${>}\mathrm{FeOH} + \mathrm{H^+} + \mathrm{C_2O_4^{2-}} = {>}\mathrm{FeO_2C_2O_2^-} + \mathrm{H_2O} \quad (17)$$

In eq 16, two surface hydroxyl groups bonded to one iron protonate to form two waters, which are then released as the surface iron bonds with two oxygens of the oxalate. In contrast, in eq 17, only one surface hydroxyl group bonded to the surface iron protonates, and only one water is released. The different reaction stoichiometries in eq 16 and 17 result in very different model predictions of adsorption. It should also be noted that the reaction stoichiometry in eq 17 is identical to that in eq 6. With the dipole model, the electrostatic work factors for the reactions in eqs 16 and 17 are $\Delta\psi_r = 0$ and $\Delta\psi_r = -\psi_\beta$, respectively. Together with the differences in reaction stoichiometry, it becomes possible to use adsorption data to distinguish between eq 16 and 17.

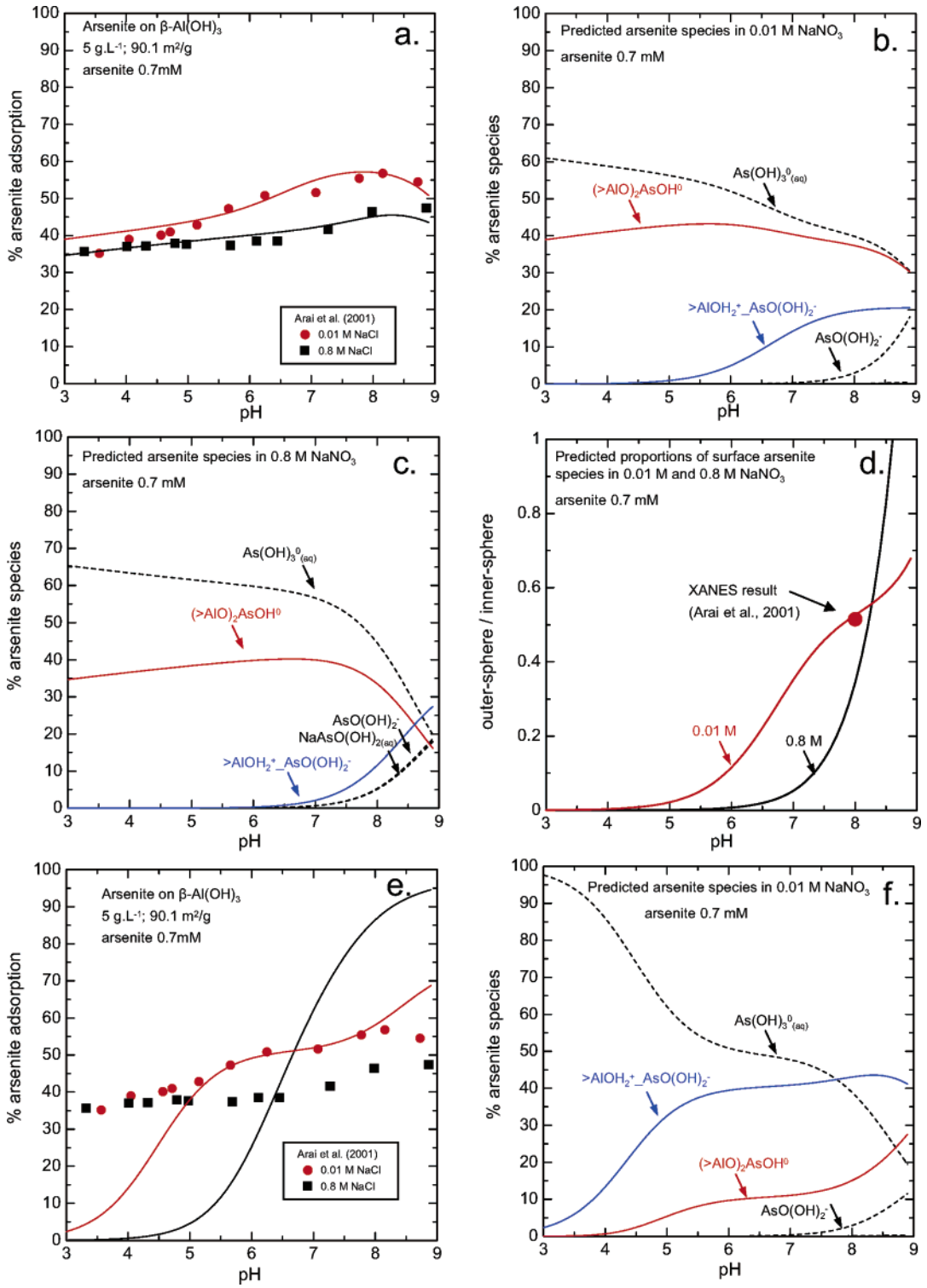

FIGURE 3. Arsenite adsorption on alumina. The curves in a−d were calculated with the dipole modification of the TLM and arsenite surface species given in eqs 11−15, log $*K^0_{(>\mathrm{AlO})_2\mathrm{As(OH)}^0} = 5.0$ ($\Delta\psi_r = 0$), log $*K^0_{>\mathrm{AlOH_2}^+\_\mathrm{AsO(OH)_2}^-} = 3.1$ ($\Delta\psi_r = \psi_0 - \psi_\beta$), Ns = 5.0 sites·nm^{-2}, log $*K_1^0 = 5.8$, log $*K_2^0 = 12.8$, log $*K^0_{\mathrm{Na}^+} = -9.9$, log $*K^0_{\mathrm{NO_3}^-} = 8.5$, and $C_1 = 0.60$ F·m^{-2}. The curves in e and f were calculated with the traditional TLM using log $*K^0_{(>\mathrm{AlO})_2\mathrm{As(OH)}^0} = 9.5$ ($\Delta\psi_r = 2\psi_0 - 2\psi_\beta$) and log $*K^0_{>\mathrm{AlOH_2}^+\_\mathrm{AsO(OH)_2}^-} = 5.0$ (see text). The surface protonation and electrolyte adsorption parameters were calculated from predicted values for gibbsite (*45*) using the experimental isoelectric point (*6*). Aqueous arsenite protonation equilibria were taken from a recent summary (*47*). We also included in the aqueous speciation model a value of log $K = 8.6$ for the reaction $\mathrm{NaAsO(OH)_2} + \mathrm{H}^+ = \mathrm{As(OH)_3} + \mathrm{Na}^+$ retrieved from high ionic strength adsorption studies (in progress). (a) Arsenite adsorption as a function of pH and ionic strength. The curves represent regression fits of the experimental data plotted as symbols (*6*). (b,c) Predicted model arsenite surface and aqueous speciation. The outer- and inner-sphere arsenite surface complexes are approximately equal in abundance only at high pH. The proportion of outer-sphere complex increases with pH, but decreases with increasing ionic strength consistent with XAFS results (*6*). (d) Predicted proportions of outer- to inner-sphere arsenite surface complexes at 0.01 and 0.8 M $NaNO_3$. The solid curve for 0.01 M agrees with the experimental XANES result at pH = 8. (e,f) The curves represent traditional TLM calculations which differ from those in a−d. solely through the use of a different electrostatic factor for the binuclear complex and different magnitudes of log *K* values (as noted above).

The solid curves in Figure 4a were generated by regression of the experimental data shown using the inner-sphere complex represented by eq 17 for which

$$K = \frac{a_{>\mathrm{FeO_2C_2O_2^-}} a_{\mathrm{H_2O}}}{a_{>\mathrm{FeOH}} a_{\mathrm{H^+}} a_{\mathrm{C_2O_4^{2-}}}} 10^{-F\psi_\beta/2.303RT} \quad (18)$$

and an unprotonated outer-sphere complex represented by

$$2 > \mathrm{FeOH} + 2\mathrm{H^+} + \mathrm{C_2O_4^{2-}} = (>\mathrm{FeOH_2^+})_2\_\mathrm{C_2O_4^{2-}} \quad (19)$$

and

$$K = \frac{a_{(>\mathrm{FeOH_2^+})_2\_\mathrm{C_2O_4^{2-}}}}{a_{>\mathrm{FeOH}}^2 a_{\mathrm{H^+}}^2 a_{\mathrm{C_2O_4^{2-}}}} 10^{2F(\psi_0-\psi_\beta)/2.303RT} \quad (20)$$

Equation 16 is not consistent with the adsorption data shown in Figure 4a. As an independent test of the model, the predicted abundances of the inner- and outer-sphere complexes as functions of pH and surface loading can be compared in Figure 4b,c with the speciation obtained experimentally by ATR−FTIR spectroscopy (*8*). The latter results are the most detailed experimental surface speciation results obtained to date for anion adsorption. They afford a far more rigorous test of predicted model speciation than the cases of sulfate and arsenite discussed above. Uncertainties in the experimental surface speciation data are not shown explicitly in Figure 4b,c but must be about ±5% below pH = 6 and about ±20% at pH > 6 (*8*). Uncertainties in the model curves result from the fact that all the electrolyte model parameters for this goethite in NaCl solutions are predicted. Additional model uncertainty arises from the regression fit to the adsorption data in Figure 4a, which may be of the order of ±0.2 log *K* unit in the surface oxalate equilibrium constants. The overall uncertainties in the model curves must be at least ±20%. It can be seen in Figure 4b,c that the model curves for the more abundant (inner-sphere) complex agree with the datapoints within the overall experimental and model uncertainties at all pH values. The agreement of the model curves for the less abundant (outer-sphere) complex with the datapoints is not as good at pH < 5, where the model would be most sensitive to the underlying electrolyte parameters (i.e. farthest from the pH_{ZPC}). It is also possible that an additional surface species may be applicable under these conditions. Considering all the uncertainties in both model predictions and the experimental data, the overall predictions of the model are in reasonable agreement with the datapoints, which strongly supports the dipole modification of the TLM. On the strength of the agreements shown in Figure 4a−c, we have made additional predictions of surface oxalate speciation on goethite at lower ionic strength (Figure 4d), where it can be seen that the outer-sphere complex can, by far, account for the bulk of oxalate adsorption at pH values of 7−8. We have also found that eqs 17−20 are nearly consistent with other oxalate/goethite bulk adsorption data referring to much wider ranges of pH, ionic strength, and surface coverage (*41, 42*), as well as adsorption data for oxalate on alumina (*43*). In the latter case, a study of infrared spectra coupled with quantum mechanical models of atomic clusters (*10*) led to the conclusion that the surface Al has increased its coordination number from 4 to 5 as it bonds with oxalate. It is interesting to note that a similar inference could be made for the surface Fe in the reaction stoichiometry of eq 17 above. Finally, model predictions of the ζ potential of goethite in oxalate solutions (assuming $\zeta = \psi_d$) show an extremely large charge-reversal effect with increasing oxalate concentration. Qualitatively, this is consistent with the direction of displacement of electrophoretic mobility data with increasing oxalate concentration (*44*).

Without the dipole modification to $\Delta\psi_r$ in eq 18, the model fit and predictions are quite different. In a TLM that takes account of ions only, eq 18 would give $\Delta\psi_r = \psi_0 - 2\psi_\beta$ for a mononuclear, bidentate complex on the β-plane. The resulting adsorption model curves and predicted speciation are shown in Figure 4e,f. It can be seen in Figure 4e that the model curves are strongly inconsistent with the adsorption data. In Figure 4f, the relative abundances of the predicted surface species are inconsistent with spectroscopic results. The large differences between panels e and f in Figure 4 compared with panels a and b are due solely to the use of $\Delta\psi_r = \psi_0 - 2\psi_\beta$ (no dipole contribution) versus $\Delta\psi_r = -\psi_\beta$ (with dipole contribution) as well as different log *K* values. It is clear in this third example that taking into account the electrostatics of water dipole desorption also has a very large effect on the performance of the surface complexation model.

The analyses of sulfate, arsenite, and oxalate adsorption using surface species established by spectroscopic studies, and the independent prediction of speciation behavior as functions of pH, ionic strength and surface coverage in agreement with spectroscopic results, strongly support the dipole modification of the TLM. The physical basis of the dipole modification is the inclusion of the electrostatic consequences of water dipole desorption during ligand-exchange reactions. In implementing the dipole modification, inner-sphere anion complexes are placed on the β-plane of the TLM and the electrostatic factor for the reaction ($\Delta\psi_r$) is changed according to the number of moles of water released by desorption from sites on the 0-plane. Outer-sphere anion complexes are also placed on the β-plane, but the electrostatic factor for the reaction ($\Delta\psi_r$) is not altered from the tradional approach because no water dipoles are released from the 0-plane. From a modeling standpoint, the advantage of this approach is its simplicity. No additional fit parameters are involved, yet an important role for the water dipole is included in the model and the model predictions are consistent with spectroscopic results.

Alternate formulations of the TLM for anion adsorption reactions are, of course, possible for the anions treated in this paper (i.e. without including the electrostatics of water dipole desorption). For example, an inner-sphere sulfate ion can be placed on the 0-plane and an outer-sphere on the β-plane yielding results almost the same as those shown in Figure 2a−d. This is a consequence of the relative unimportance of the inner-sphere sulfate species compared to the outer-sphere species in Figure 2a−d. Such a model, however, does not describe all other sets of sulfate data. For arsenite, it can be recognized that using an inner-sphere complex on the 0-plane and the same outer-sphere complex on the β-plane used above results in the same formal reactions. The electrostatic factors and results are shown in Figure 3a−d. This is a consequence of $\Delta\psi_r$ being equal to zero in the latter model as well as in the dipole model. In contrast, for oxalate, an inner-sphere complex on the 0-plane and the same outer-sphere complex on the β-plane used above results in a poorer description of the adsorption data in Figure 4a−c. Overall, the dipole modification of the TLM used here gives the best fit to the largest body of adsorption data, consistent with spectroscopic results. Its predictions can be expected to differ the most from those implementations of the TLM without considerations of a dipole contribution when an inner-sphere surface species with $\Delta\psi_r$ not equal to zero is the most abundant species. For example, TLM studies of inner-sphere binuclear bidentate arsenate on hematite without a dipole contribution (e.g. $\Delta\psi_r = -\psi_0$) are not consistent with the adsorption data (*17*). However, the same study demonstrated that $\Delta\psi_r = -\psi_\beta$ is consistent with the adsorption data. Although this result was interpreted in terms of a charge distribution, it could also be interpreted as a consequence of the electrostatic contribution from the

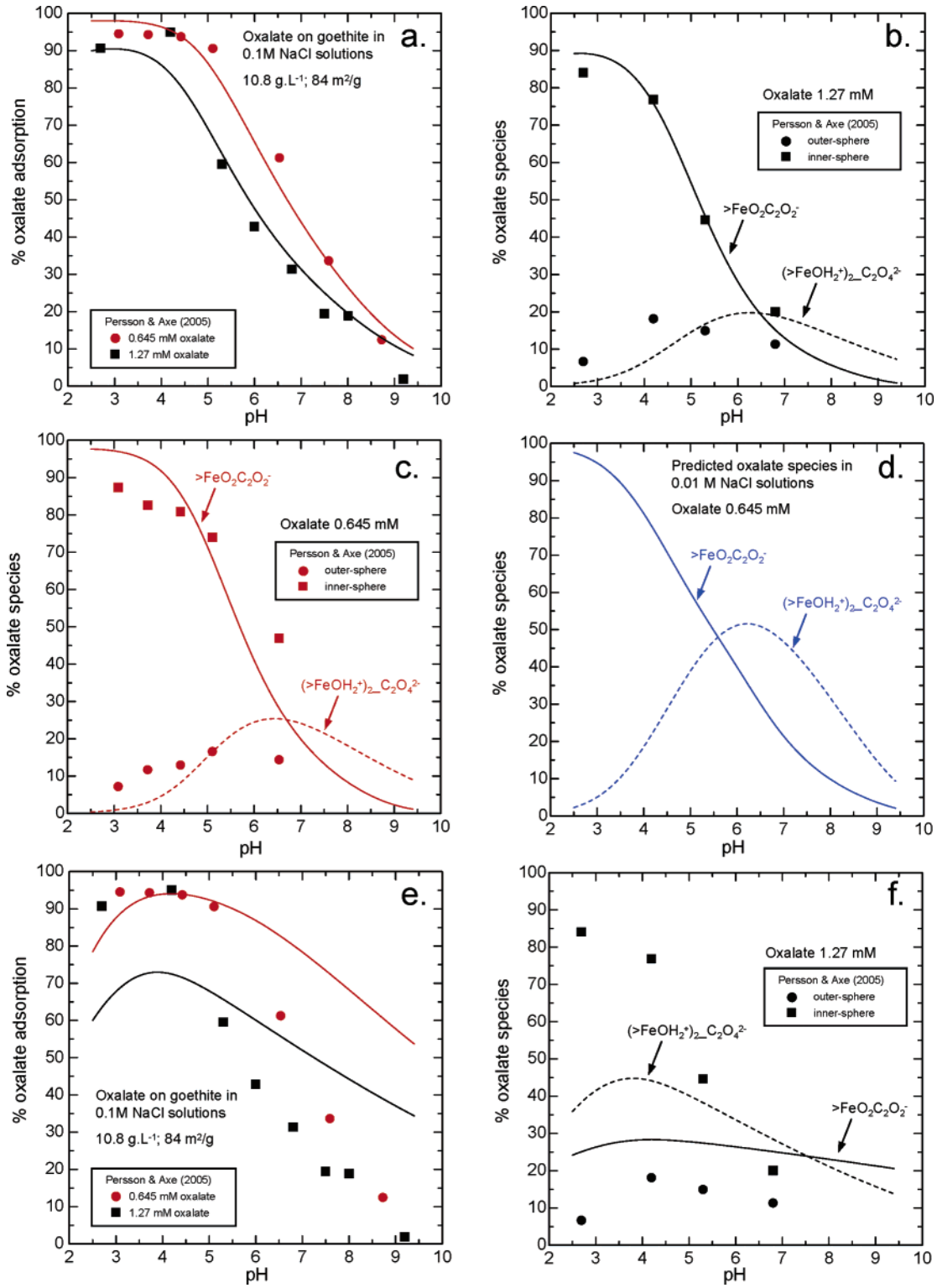

FIGURE 4. Oxalate adsorption on goethite. The curves in a–d were calculated with the dipole modification of the TLM using oxalate surface species given in eq 17–20, log $^*K^0_{>FeO_2C_2O_2^-} = 10.7$ ($\Delta\psi_r = -\psi_\beta$), log $^*K^0_{(>FeOH_2^+)_2\_C_2O_4^{2-}} = 23.1$ ($\Delta\psi_r = 2\psi_0 - 2\psi_\beta$), log $^*K_1^0 = 6.1$, log $^*K_2^0 = 12.3$, log $^*K^0_{Na^+} = -8.9$, log $^*K^0_{Cl^-} = 9.3$, and $C_1 = 0.72$ F·m^{-2}. The curves in e and f were calculated with the traditional TLM using log $^*K^0_{>FeO_2C_2O_2^-} = 14.3$ ($\Delta\psi_r = \psi_0 - 2\psi_\beta$) and log $^*K^0_{(>FeOH_2^+)_2\_C_2O_4^{2-}} = 24.3$ (see text). The surface protonation and electrolyte adsorption parameters were calculated from predicted values (*45*) consistent with the site density of 2.5 sites·nm^{-2} (based on preliminary fits as a function of suface coverage). Aqueous oxalate protonation constants and a Na-oxalate ion-pair constant were taken from a recent report (*48*). (a) Oxalate adsorption as a function of pH and surface coverage at 0.1 M NaCl. The curves represent regression fits of the experimental data plotted as symbols (*8*). (b,c) Predicted model oxalate surface speciation at 0.1 M NaCl. The outer- and inner-sphere oxalate surface complexes are approximately equal in abundance at pH ≈ 7–8. At both surface coverages, within the overall experimental and model uncertainties, the predicted relative abundances of the inner- and outer-sphere complexes compare favorably with the ATR–FTIR results (*8*). (d) Predicted model oxalate surface speciation at 0.01 M NaCl. The outer-sphere complex is predicted to predominate at pH values of 7–8. (e,f) The curves represent traditional TLM calculations which differ from those in a–d. solely through the use of a different electrostatic factor for the mononuclear complex and different magnitudes of log *K* values (as noted above).

desorption of two moles of water dipoles, i.e., $\Delta\psi_r = 2\psi_0 - 3\psi_\beta - 2(\psi_0 - \psi_\beta) = -\psi_\beta$.

The predictions of the dipole modification of the TLM agree with the spectroscopic results because including the water dipole in $\Delta\psi_r$ apparently produces the appropriate electrostatic potential changes for inner-sphere surface complexation. In addition, the dipole modification results in increased sensitivity to alternate possible surface speciation schemes because no additional fit parameters are involved. These features make it possible to establish additional details of the stoichiometry of adsorption reactions. For example, the protonation states of the surface species can be established when these are not known from infrared (or X-ray) spectroscopy. In this way, the modified triple-layer surface complexation model becomes a useful tool, not only for the integration of spectroscopic and bulk adsorption data, but also for making predictions of surface speciation over wide ranges of conditions of relevence to the migration of toxic species in the environment.

Acknowledgments

We greatly appreciate discussions with Y. Arai, J. A. Davis, D. B. Kent, and G. A. Waychunas. We also thank J. C. McIntosh, D. L. Sparks, J. Hering, and two journal reviewers for reading the manuscript and making useful suggestions. Financial support was provided by DOE Grant DE-FG02-96ER-14616.

Literature Cited

(1) Dixit, S.; Hering, J. G. Comparison of arsenic(V) and arsenic (III) sorption onto iron oxide minerals: implications for arsenic mobility. *Environ. Sci. Technol.* **2003**, *37*, 4182−4189.

(2) Drever, J. I. *The geochemistry of natural waters*, 3rd ed.; Prentice Hall: Upper Saddle River, NJ, 1997.

(3) Kraemer, S. M. Iron oxide dissolution and solubility in the presence of siderophores. *Aquat. Sci.* **2004**, *66*, 3−18.

(4) Connor, P. A.; McQuillan, A. J. Phosphate adsorption onto TiO2 from aqueous solutions: an in situ internal reflection infrared spectroscopic study. *Langmuir* **1999**, *15*, 2916−2921.

(5) Hazen, R. M.; Sholl, D. S. Chiral selection on inorganic crystal surfaces. *Nature* **2003**, *2*, 367−373.

(6) Arai, Y.; Elzinga, E.; Sparks, D. L. X-ray absorption spectroscopic investigation of arsenite and arsenate adsorption at the aluminum oxide-water interface. *J. Colloid Interface Sci.* **2001**, *235*, 80−88.

(7) Peak, D.; Ford, R. G.; Sparks, D. L. An in situ ATR-FTIR investigation of sulfate bonding mechanisms on goethite. *J. Colloid Interface Sci.* **1999**, *218*, 289−299.

(8) Persson, P.; Axe, K. Adsorption of oxalate and malonate at the water-goethite interface: molecular surface speciation from IR spectroscopy. *Geochim. Cosmochim. Acta* **2005**, *69*, 541−552.

(9) Johnson, B. B.; Sjoberg, S.; Persson, P. Surface complexation of mellitic acid to goethite: an attenuated total reflection Fourier transform infrared study. *Langmuir* **2004**, *20*, 823−828.

(10) Yoon, T. H.; Johnson, S. B.; Musgrave, C. B.; Brown, G. E., Jr. Adsorption of organic matter at mineral/water interfaces: I. ATR-FTIR spectroscopic and quantum chemical study of oxalate adsorbed at boehmite/water and corundum/water interfaces. *Geochim. Cosmochim. Acta* **2004**, *68*, 4505−4518.

(11) Suarez, D. L.; Goldberg, S.; Su, C. In *Mineral−Water Interfacial Reactions: Kinetics and Mechanisms*; Sparks, D. L., Grundl, T. J., Eds.; ACS Symposium Series 715, American Chemical Society: Washington, DC, 1998; pp 136−178.

(12) Hiemstra, T.; van Riemsdijk, W. H. Surface structural ion adsorption modeling of competitive binding of oxyanions by metal (hydr)oxides. *J. Colloid Interface Sci.* **1999**, *210*, 182−193.

(13) Blesa, M. A.; Weisz, A. D.; Morando, P. J.; Salfity, J. A.; Magaz, G. E.; Regazzoni, A. E. The interaction of metal oxide surfaces with complexing agents dissolved in water. *Coord. Chem. Rev.* **2000**, *196*, 31−63.

(14) Goldberg, S.; Johnston, C. T. Mechanisms of arsenic adsorption on amorphous oxides evaluated using macroscopic measurements, vibrational spectroscopy, and surface complexation modeling. *J. Colloid Interface Sci.* **2001**, *234*, 204−216.

(15) Richter, A.; Brendler, V.; Nebelung, C. Blind prediction of Cu(II) sorption onto goethite: current capabilities of diffuse double layer model. *Geochim. Cosmochim. Acta* **2005**, *69*, 2725−2734.

(16) Davis, J. A.; Meece, D. E.; Kohler, M.; Curtis, G. P. Approaches to surface complexation modeling of uranium (VI) adsorption on aquifer sediments. *Geochim. Cosmochim. Acta* **2004**, *68*, 3621−3642.

(17) Arai, Y.; Sparks, D. L.; Davis, J. A. Effects of dissolved carbonate on arsenate adsorption and surface speciation at the hematite-water interface. *Environ. Sci. Technol.* **2004**, *38*, 817−824.

(18) Villalobos, M.; Leckie, J. O. Surface complexation modeling and FTIR study of carbonate adsorption to goethite. *J. Colloid Interface Sci.* **2001**, *235*, 15−32.

(19) Dzombak, D. A.; Morel, F. M. M. *Surface Complexation Modeling*; John Wiley and Sons: New York, 1990.

(20) Criscenti, L. J.; Sverjensky, D. A. A single-site model for divalent and heavy metal adsorption over a range of metal concentrations. *J. Colloid Interface Sci.* **2002**, *253*, 329−352.

(21) Sverjensky, D. A.; Sahai, N. Theoretical prediction of single-site surface protonation equilibrium constants for oxides and silicates in water. *Geochim. Cosmochim. Acta* **1996**, *60*, 3773−3798.

(22) James, R. O.; Healy, T. W. Adsorption of hydrolyzable metal ions at the oxide-water interface III. A thermodynamic model of adsorption. *J. Colloid Interface Sci.* **1972**, *40*, 65−81.

(23) Yates, D. E.; Levine, S.; Healy, T. W. Site-binding model of the electrical double layer at the oxide/water interface. *J. Chem. Soc., Faraday Trans.* **1974**, *70*, 1807−1818.

(24) Huang, C.; Stumm, W. Specific Adsorption of Cations on Hydrous γ-Al2O3. *J. Colloid Interface Sci.* **1973**, *43*, 409−420.

(25) Schindler, P. W. In *Adsorption of Inorganics at Solid-Liquid Interfaces*; Anderson, M. A., Rubin, A. J., Eds.; Ann Arbor Science Publishers: Ann Arbor, MI, 1981; pp 1−47.

(26) Davis, J. A.; Leckie, J. O. Surface ionization and complexation at the oxide/water interface 3. Adsorption of anions. *J. Colloid Interface Sci.* **1980**, *74*, 32−43.

(27) Hiemstra, T.; van Riemsdijk, W. H. A surface structural approach to ion adsorption: The charge distribution (CD) model. *J. Colloid Interface Science* **1996**, *179*, 488−508.

(28) Stumm, W. *Chemistry of the Solid-Water Interface*; John Wiley and Sons., Inc.: New York, 1992.

(29) Bockris, J. O. M.; Reddy, A. K. N. *Modern Electrochemistry*; Plenum Press: New York, 1970; Vol. 2.

(30) Grossl, P.; Eick, M. J.; Sparks, D. L.; Goldberg, S.; Ainsworth, C. C. Arsenate and chromate retention mechanisms on goethite. 2. Kinetic evaluation using a pressure-jump relaxation technique. *Environ. Sci. Technol.* **1997**, *31*, 321−326.

(31) Zhang, P. C.; Sparks, D. L. Kinetics and mechanisms of molybdate adsorption/desorption at the goethite/water interface using pressure-jump relaxation. *Soil Sci. Soc. Am. J.* **1990**, *53*, 1028−1034.

(32) Badyal, Y. S.; Saboungi, M.-L.; Price, D. L.; Shastri, S. D.; Haeffner, D. R. Electron distribution in water. *J. Chem. Phys.* **2000**, *112*, 9206−9208.

(33) Sverjensky, D. A. Interpretation and prediction of triple-layer model capacitances and the structure of the oxide-electrolyte-water interface. *Geochim. Cosmochim. Acta* **2001**, *65*, 3641−3653.

(34) Myneni, S. In *Sulfate Minerals - Crystallography*; Alpers, C. N., Jambor, J. L., Nordstrom, D. K., Eds.; Mineralogical Society of America: Washington, DC, 2000; Vol. 40, pp 113−172.

(35) Wijnja, H.; Schulthess, C. P. Vibrational spectroscopy study of selenate and sulfate adsorption mechanisms on Fe and Al (Hydr)oxide surfaces. *J. Colloid Interface Sci.* **2000**, *229*, 286−297.

(36) Ali, M. A.; Dzombak, D. A. Competitive adsorption of simple organic acids and sulfate on goethite. *Environ. Sci. Technol.* **1996**, *30*, 1061−1071.

(37) Rietra, R. P. J. J.; Hiemstra, T.; van Riemsdijk, W. H. Comparison of selenate and sulfate adsorption on goethite. *J. Colloid Interface Sci.* **2001**, *240*, 384−390.

(38) Yates, D. E.; Healy, T. W. Mechanism of anion adsorption at the ferric and chromic oxide/water interfaces. *J. Colloid Interface Sci.* **1975**, *52*, 222−228.

(39) Rietra, R. P. J. J. The relation between molecular structure and ion adsorption on goethite; Ph.D. Thesis, Wageningen University, 2001.

(40) Hansmann, D. D.; Anderson, M. A. Using electrophoresis in modeling sulfate, selenite, and phosphate adsorption onto goethite. *Environ. Sci. Technol.* **1985**, *19*, 544−551.

(41) Mesuere, K.; Fish, W. Chromate and oxalate adsorption on goethite. 1. Calibration of surface complexation models. *Environ. Sci. Technol.* **1992**, *26*, 2357−2364.

(42) Mesuere, K.; Fish, W. Chromate and oxalate adsorption on goethite. 2. Surface complexation modeling of competitive adsorption. *Environ. Sci. Technol.* **1992**, *26*, 2365−2370.
(43) Johnson, S. B.; Yoon, T. H.; Kokar, B. D.; Brown, G. E., Jr. Adsorption of organic matter at mineral/water interfaces: 3. Implications of surface dissolution for adsorption of oxalate. *Langmuir* **2004**, *20*, 11480−11492.
(44) Djafer, M.; Khandal, R. K.; Terce, M. Interactions between different anions and the goethite surface as seen by different methods. *Colloids Surf.* **1991**, *54*.
(45) Sverjensky, D. A. Prediction of surface charge on oxides in salt solutions: revisions for 1: 1 (M+L-) electrolytes. *Geochim. Cosmochim. Acta* **2005**, *69*, 225−257.
(46) Ali, M. A.; Dzombak, D. A. Interaction of Cu, organic acids and sulfate in goethite suspensions. *Geochim. Cosmochim. Acta* **1996**, *60*, 5045−5053.
(47) Nordstrom, D. K.; Archer, D. G. Arsenic thermodynamic data and environmental geochemistry. In *Arsenic in Ground Water: Geochemistry and Occurrence*; Welch, A. H., Stollenwerk, K. G., Eds.; Kluwer Academic Publishers: Boston, 2003; pp 1−25.
(48) Smith, R. M.; Martell, A. E. *NIST Critically Selected Stability Constants of Metal Complexes Database*; U. S. Department of Commerce, Technology Administration: U.S. Governement Printing Office: Washington, DC, 2004.

Received for review August 2, 2005. Revised manuscript received October 25, 2005. Accepted October 31, 2005.

ES051521V